

Graphitic Carbon Nitride as a Photovoltaic Booster in Quantum Dot Sensitized Solar Cells: A Synergistic Approach for Enhanced Charge Separation and Injection

Tridip Ranjan Chetia,^a Mohammad Shaad Ansari,^a and Mohammad Qureshi^{*a}

^aMaterials Science Laboratory, Department of Chemistry, Indian Institute of Technology Guwahati, Assam, 781039, India.

*E-mail: mq@iitg.ernet.in, Tel.: +91-361-2582320. Fax: +91-361-2582349

1. Energy-dispersive X-ray spectroscopy (EDX) maps and patterns of the (g-C₃N₄-ZnO NR) composite.

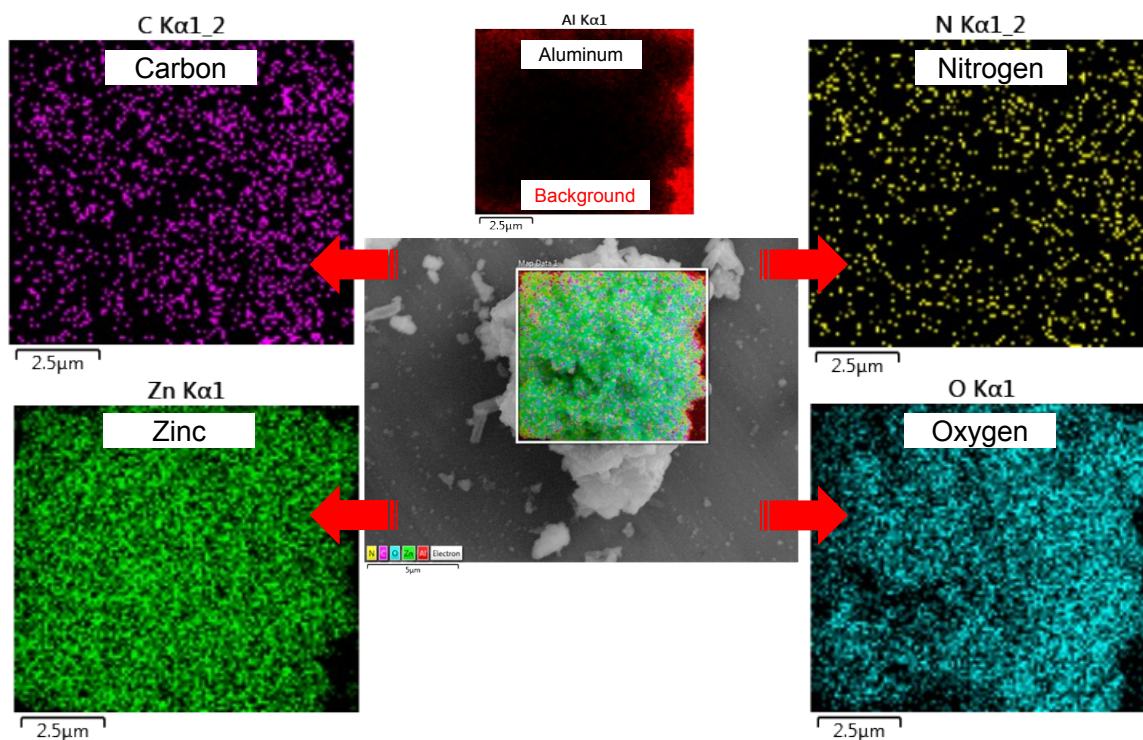


Figure S1. Energy-dispersive X-ray spectroscopy (EDX) maps of the hybrid composite (g-C₃N₄-ZnO NR) with optimum weight ratio [i.e., (0.5:1)].

To elucidate elemental distribution and composition in (g-C₃N₄-ZnO NR) composite with weight ratio (0.5:1), selected area elemental mapping is performed by energy dispersive X-ray (EDX) spectroscopic technique and depicted in the figure S1. Homogeneous distribution of all the elements [i.e., Carbon (C), Nitrogen (N), Zinc (Zn) and Oxygen (O)] throughout the whole composite is observed from the EDX maps. This observation confirms successful incorporation of g-C₃N₄ sheets with the ZnO NRs and hence preparation of the composite.

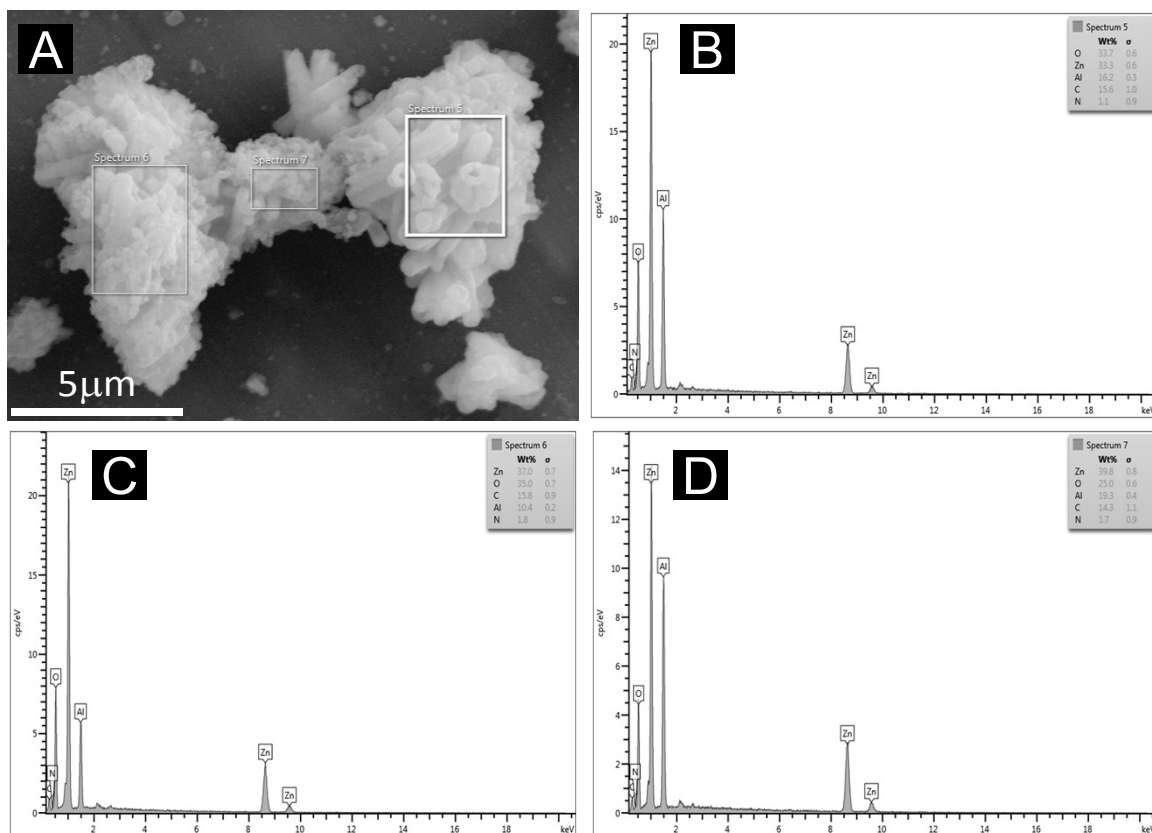


Figure S2. (A) FESEM image of the (g-C₃N₄-ZnO NR) composite with optimum weight ratio [i.e., (0.5:1)] indicating the areas used for recording energy-dispersive X-ray (EDX) patterns (B), (C), and (D) respectively.

Figure S2 represents EDX patterns for the composite, recorded in different parts of the sample as indicated in the FESEM image (A). EDX patterns [(B), (C) and (D)] further validates the existence of all the elements namely, C, N, Zn and O in the composite and confirms purity of the sample. Please note that, peaks for aluminum (Al) are observed due to the background aluminum foil used for deposition of the sample. Inset to the EDX patterns show elemental compositions (wt %) contained in the composite which are in well agreement with the weight ratio of the sample [i.e., (0.5:1); g-C₃N₄ to ZnO NR].

2. Time resolved photoluminescence (PL) spectra for all the composites.

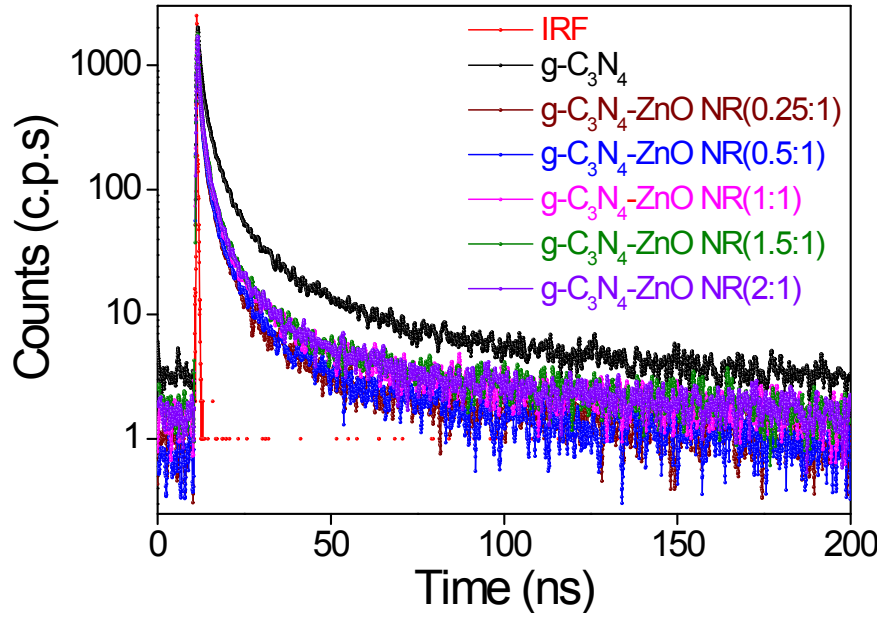


Figure S3. Dynamic PL spectra for all the (g-C₃N₄-ZnO NR) composites and pristine g-C₃N₄ sheets recorded at an excitation wavelength of 350 nm.

Table S1. Calculated parameters such as fitting parameter (χ^2), exciton lifetimes (τ_1 , τ_2 , τ_3), pre-exponential factors (α_1 , α_2 , α_3), average exciton lifetimes ($\langle\tau\rangle$) are summarized in the following table:

Sample	χ^2	τ_1 (ns)	τ_2 (ns)	τ_3 (ns)	α_1	α_2	α_3	$\langle\tau\rangle$ (ns)
g-C ₃ N ₄	1.055	0.831	3.6	19.094	36.50	41.01	22.49	14.41
(0.25:1)	0.935	0.210	1.324	6.855	32.22	44.98	22.80	5.17
(0.5:1)	0.941	0.831	1.275	6.766	31.13	43.86	25.01	5.27
(1:1)	0.968	0.351	2.091	11.497	35.32	44.35	20.32	8.51
(1.5:1)	0.972	0.358	2.066	11.285	36.18	43.44	43.44	8.37
(2:1)	0.974	0.318	1.995	1.995	35.27	44.69	20.04	8.60

3. PXRD pattern of as synthesized ZnO heterostructures (NP and NR) and their g-C₃N₄ composites.

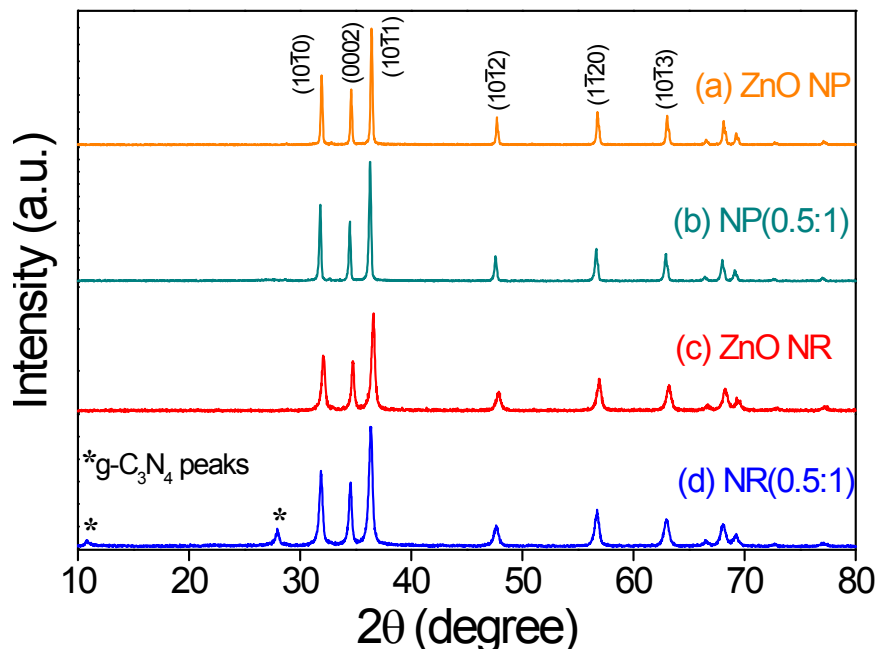


Figure S4. PXRD patterns for (a) pristine ZnO NP, (b) NP (0.5:1) [(g-C₃N₄-ZnO NP) composite], (c) pristine ZnO NR and (d) NR (0.5:1) [(g-C₃N₄-ZnO NR) composite].

Figure S4 illustrates powder X-ray diffraction (PXRD) patterns for as synthesized pristine ZnO NP, ZnO NR and their composites with g-C₃N₄. Trace (a) and (c) are the PXRD patterns of pristine ZnO NPs and ZnO NRs which are defined to be wurtzite hexagonal crystal phase with a $P6_3mc$ space group symmetry according to the JCPDS Card No. 36-1451. Traces (b) and (d) are the PXRD patterns for the composite (g-C₃N₄-ZnO NP) and (g-C₃N₄-ZnO NR) respectively having g-C₃N₄ to ZnO weight ratio (0.5:1). In the PXRD pattern of (g-C₃N₄-ZnO NR) composite [trace (d)], two low intense peaks at $2\theta \approx 11.2^\circ$ and 27.5° are observed for amorphous g-C₃N₄ sheets. However, in the trace (b) for ZnO NP based g-C₃N₄ composite, characteristic peaks for g-C₃N₄ are not visible which might be due to low scattering power of amorphous g-C₃N₄ sheets relative to the ZnO NPs. It should be noted that diffraction peaks for as synthesized ZnO NPs are sharp and intense as compared to the ZnO NRs.

4. Diffuse reflectance UV-visible absorption spectra of as synthesized ZnO heterostructures and their g-C₃N₄ composites.

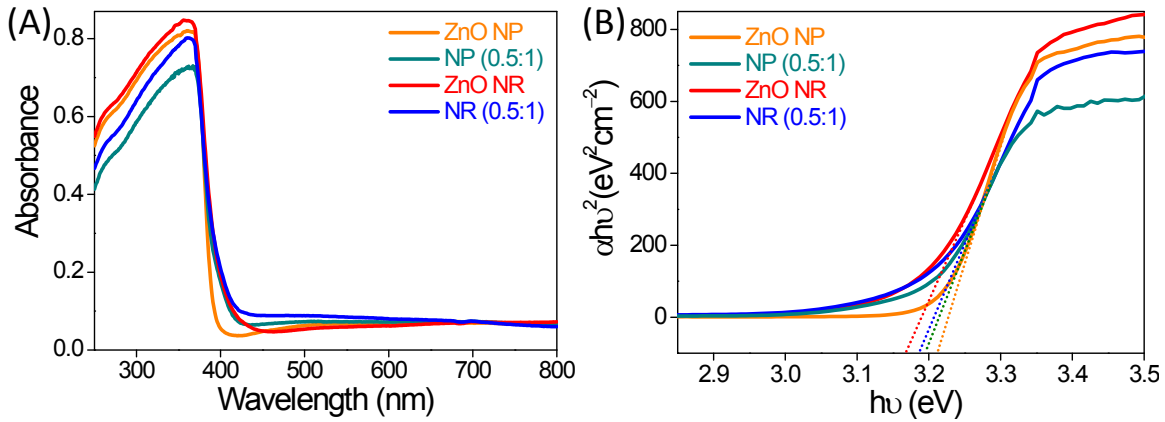


Figure S5. (A) Diffuse reflectance UV-visible (UV-vis) absorption profiles for as synthesized pristine ZnO NP, ZnO NR and their composites of g-C₃N₄ with a weight ratio (0.5:1). (B) Corresponding Tauc plots for estimation of optical band gap values.

Figure S5 (A) shows diffuse reflectance UV-visible (UV-vis) absorption spectra of as synthesized pristine materials, i.e., ZnO NP (orange line) and ZnO NR (red line) and their g-C₃N₄ composites namely, NP (0.5:1) [dark cyan line] and NR (0.5:1) [blue line]. g-C₃N₄ to ZnO weight ratio in both the composites is (0.5:1). The absorption onsets for each sample are well correlated with the optical band gap values which are estimated from corresponding Tauc plot, as shown in figure S5 (B). The optical band gap values are found to be ~3.21 eV for ZnO NP, ~3.17 for ZnO NR whilst for the g-C₃N₄ composites of ZnO NP and ZnO NR they are ~3.19 eV and ~3.18 eV respectively.

5. Fourier Transform Infrared (FT-IR) analyses.

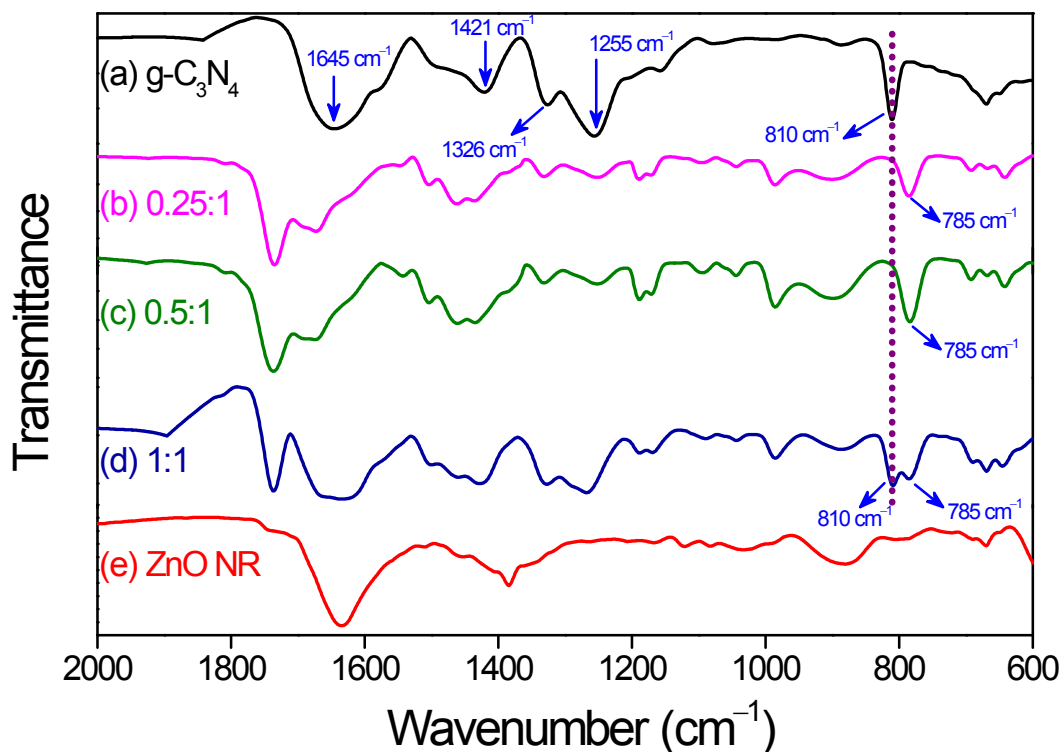


Figure S6. FT-IR spectra of (a) pristine g-C₃N₄, (g-C₃N₄-ZnO NR) composite weight ratios namely, (b) 0.25:1, (c) 0.5:1 (d) 1:1 and for (e) pristine ZnO nanorods (NR).

Figure S6 shows FT-IR spectra for (a) pristine g-C₃N₄ (black line); (g-C₃N₄-ZnO NR) composite weight ratios namely, (b) 0.25:1 (magenta line), (c) 0.5:1 (olive line) and (d) 1:1 (navy blue line) as well as for (e) pristine ZnO nanorods (NR) (red line). In the FT-IR spectrum of pristine g-C₃N₄, trace (a), dominating peaks centered at 1255 cm⁻¹, 1326 cm⁻¹ and 1421 cm⁻¹ are corresponding to C-N stretching vibration modes while the broad peak centered at ~1645 cm⁻¹ is attributed to C=N stretching vibrations.¹ In addition, the peak observed at 810 cm⁻¹ is due to the characteristic out-of-plane bending modes of *s*-triazine repeating units of g-C₃N₄ sheets.² All the characteristic peaks of g-C₃N₄ and ZnO NR can be seen clearly in the spectra of (g-C₃N₄-ZnO NR) hybrid composites. It is observed that, the peaks of g-C₃N₄ are suppressed and broadened in the (g-C₃N₄-ZnO NR) hybrid composites. Moreover, the peak of *s*-triazine unit is shifted towards the lower wavenumber for the composite ratios (0.25:1) and (0.5:1) which is indicative of an electronic interaction between ZnO and the *s*-triazine units.³ This electronic interaction may be of great significance to transfer charge carriers and induce a synergetic effect between g-C₃N₄ sheets and ZnO NRs in the hybrid material. It should be noted that, in case of composite ratio (1:1), the characteristic peak of

s-triazine unit is appeared as a doublet and the peaks for C–N as well as C=N are observed to be prominent than the other two composite ratios namely, (0.5:1) and (0.25:1). This observation suggests that a significant number of g-C₃N₄ sheets are remain unbound to the ZnO NRs in the composite ratio (1:1) due to high content of g-C₃N₄. Hence, FT-IR analyses demonstrates that an electronic conjugation is built between g-C₃N₄ and ZnO NR in the hybrid composite which in accordance with the inferences carried out from dynamic PL studies.

6. Steady state and time resolved PL analyses of pristine g-C₃N₄ and ZnO composites.

A comparative study of excited state electronic interaction between g-C₃N₄ and ZnO in (g-C₃N₄–ZnO NP) and (g-C₃N₄–ZnO NR) composites is discussed from steady state and dynamic PL analyses.

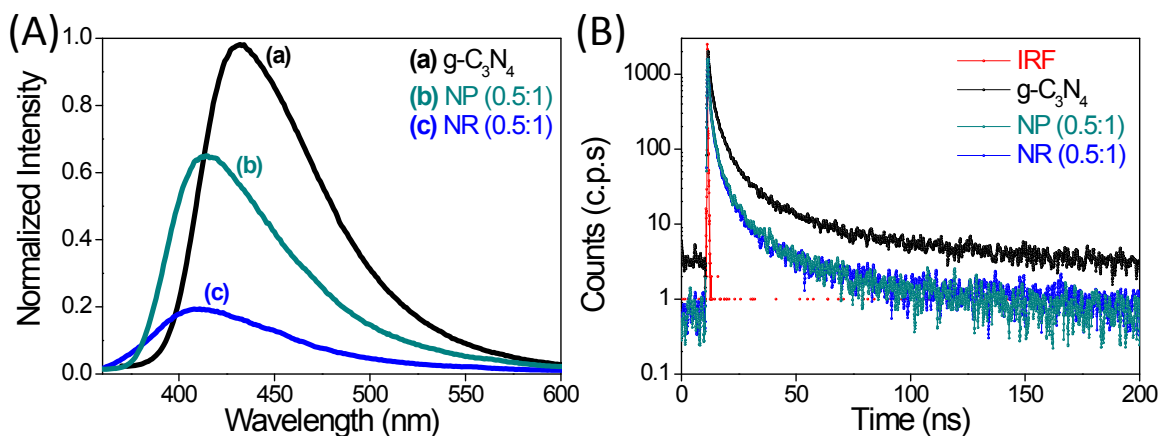


Figure S7. (A) Steady state photoluminescence (PL) spectra of (a) pure g-C₃N₄ and its composites of ZnO NP; (b) NP (0.5:1), and ZnO NR; (c) NR (0.5:1) respectively. (B) Corresponding dynamic PL spectra for the samples.

Figure S7 (A) shows steady state PL spectra for pure g-C₃N₄ (black line) and its composites of ZnO NP and ZnO NR with a weight ratio, (0.5:1); namely NP (0.5:1), [dark cyan line] and NR (0.5:1), [blue line] respectively, recorded at an excitation wavelength of 350 nm. The intensity of characteristic PL emission peak at around 432 nm for g-C₃N₄ sheets is observed to be quenched for both the composites which confirms excited state electronic interaction between ZnO and g-C₃N₄ sheets; might be due to favorable photoexcited charge transfer from g-C₃N₄ to ZnO.⁴ However, PL intensity gets more quenched in case of the ZnO NR (0.5:1) composite [NR (0.5:1), trace (c)] as compared to the ZnO NP, [NP (0.5:1), trace (b)]; possibly due to better synergistic effects between ZnO NR and g-C₃N₄. Blue shift of the emission peak (~20 nm) is also observed for the g-C₃N₄ composite of ZnO NP, as we have seen in case of (g-C₃N₄–ZnO NR) composites.

Synergistic effects in the composites are further analyzed by dynamic PL spectroscopy technique. Figure S7 (B) shows dynamic PL spectra for all the samples. We have fitted all the spectra with a tri-exponential function using fast software provided by Edinburgh instruments to calculate the exciton lifetime values. The values of fitting parameter (χ^2) and detailed spectroscopic results such as, exciton lifetimes (τ_1, τ_2, τ_3), pre-exponential factors ($\alpha_1, \alpha_2, \alpha_3$), average exciton lifetimes ($\langle\tau\rangle$) and calculated rate constants of electron injection (k_{ei}) are summarized in the table S2.

Table S2. Calculated parameters such as fitting parameter (χ^2), exciton lifetimes (τ_1, τ_2, τ_3), pre-exponential factors ($\alpha_1, \alpha_2, \alpha_3$), average exciton lifetimes ($\langle\tau\rangle$), the rate constants of electron injection (k_{ei}) are summarized in the following table:

Sample	χ^2	τ_1 (ns)	τ_2 (ns)	τ_3 (ns)	α_1	α_2	α_3	$\langle\tau\rangle$ (ns)	k_{ei} (s^{-1})
g-C₃N₄	1.055	0.831	3.600	19.094	36.50	41.01	22.49	14.41	-----
NR (0.5:1)	0.958	0.440	1.954	9.103	58.65	28.07	13.29	5.30	1.18×10^8
NP (0.5:1)	0.941	0.831	1.275	6.766	31.13	43.86	25.01	6.05	0.96×10^8

From table S2, it is clear that the average life time ($\langle\tau\rangle$) values are decreased substantially for both the composites namely, NR (0.5:1) and NP (0.5:1) as compared to g-C₃N₄, which confirms favorable photoexcited charge transfer from g-C₃N₄ sheets to ZnO. Faster and efficient charge transfer in the ZnO NR based composite than in ZnO NP composite is divulged through the minimum ($\langle\tau\rangle$) value estimated for ZnO NR composite. To authenticate our claim of faster charge migration from g-C₃N₄ sheets to ZnO NR, we have calculated the rate constants of electron injection (k_{ei}) for both the composites considering photoexcited electron transfer is the only pathway for deactivation of excited g-C₃N₄ sheets. From table S2, the k_{ei} value for the ZnO NR based composite is found to be higher ($\sim 1.18 \times 10^8$) s^{-1} than the ZnO NP composite ($\sim 0.96 \times 10^8$) s^{-1} which confirms faster photogenerated charge transfer from g-C₃N₄ sheets to ZnO NR. From all aforementioned discussions it is implicit that excited state electronic interaction between g-C₃N₄ sheets and ZnO NRs is stronger compared to ZnO NPs.

7. Steady state PL analyses of as synthesized ZnO NRs and ZnO NPs.

Emission characteristics and density of defect states in both the ZnO heterostructures are analyzed from steady state PL analyses. Figure S8 shows steady state PL spectra for ZnO NRs and ZnO NPs recorded at an excitation wavelength ~ 355 nm. The steady state PL spectra for both the samples comprises of multiple emission peaks. The sharp emission peaks in the UV range (~ 395 nm) are for near band edge emissions.⁵ The satellite peaks observed in the range of (420–500) nm are originating from the co-ordinatively unsaturated Zn^{2+} interstitial sites (Zn_i , shallow donor) whilst the emission peaks observed in the broad visible region (i.e., 500-650 nm) are accredited to the transitions from the conduction band to the deep trap levels of ZnO (created by oxygen vacancies in the ZnO crystal structure, O_i).^{5, 6}

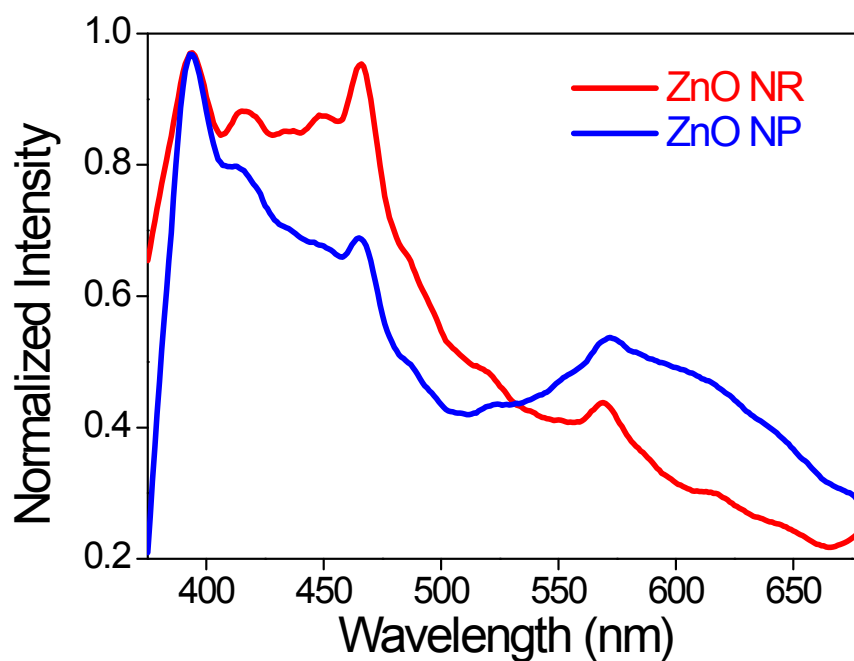


Figure S8. Steady state PL spectra of as synthesized ZnO NRs and ZnO NPs after calcination.

From figure S8, we have seen that the satellite peaks which are originating from Zn^{2+} vacancies in the ZnO crystal structures are sharp and intense for ZnO NRs (red line) compared the ZnO NPs (blue line). This observation infers higher density of Zn^{2+} defect sites in ZnO NRs. However, the intensity of broad emission band in the visible region (~ 500 -650 nm) is higher in case of ZnO NPs than the ZnO NRs which is a clear reflection of higher density of oxygen stoichiometric defect sites in as synthesized ZnO NPs.

8. Diffuse reflectance UV-vis absorption spectra for CdS QD sensitized ZnO NP and ZnO NR photoanodes

To compare CdS QD loading in the ZnO NP and ZnO NR based photoanodes we have performed diffuse reflectance UV-Vis analyses and the corresponding spectra are compiled in figure S9. From figure S9, the orange colored spectrum is for pristine ZnO NP-CdS photoanode, the red colored spectrum is for pristine ZnO NR-CdS photoanode, the dark cyan colored spectrum is for NP (0.5:1)-CdS photoanode and the blue spectrum is for NR (0.5:1)-CdS photoanode.

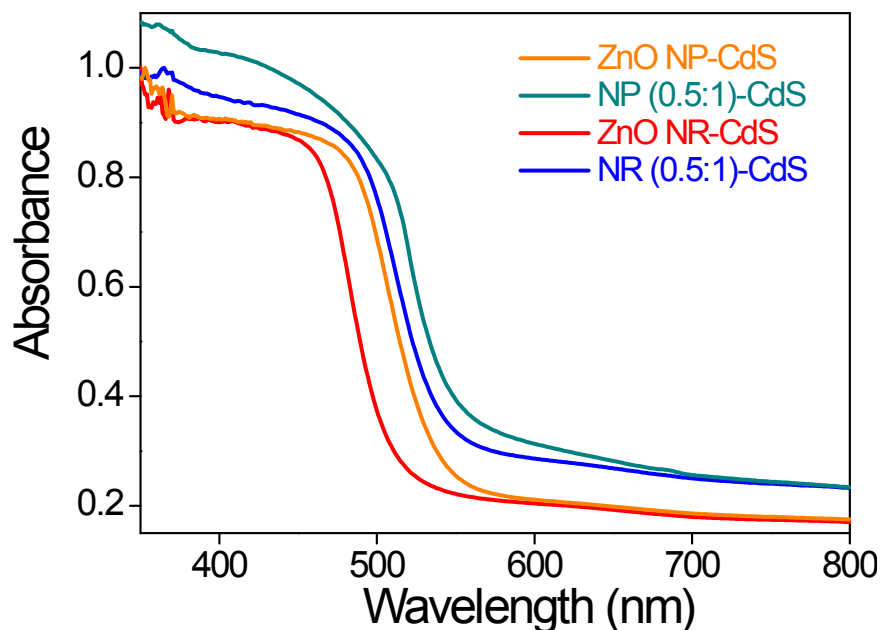


Figure S9. Diffused reflectance UV-vis spectra of CdS sensitized ZnO NP and ZnO NR based photoanodes.

As we have seen from figure S9, the absorption onsets of CdS QD sensitized ZnO NP based photoanodes [both pristine ZnO NP-CdS and NP (0.5:1) composite photoanodes] are red shifted as compared to the ZnO NR based photoanodes. This observation confirms higher loading of CdS QDs and their subsequent growth in ZnO NP based photoanodes than in the ZnO NR based photoanodes; probably due to higher specific surface area provided by the ZnO NPs. Note that, we have performed five SILAR cycles for all the photoanodes. Specific surface area for the photoanodic materials are compared by performing BET surface analyses and discussed in later.

9. BET surface area analyses of pristine ZnO NP, ZnO NR and their g-C₃N₄ composites

Figure S10 (A) depicts N₂ adsorption and desorption isotherms for pristine g-C₃N₄ [black line], ZnO NP [orange line], ZnO NR [red line], and for the composites namely NP (0.5:1) [dark cyan line], and NR (0.5:1) (Blue line). Figure S10 (B) shows corresponding Barrett–Joyner–Halenda (BJH) pore size distribution plots.

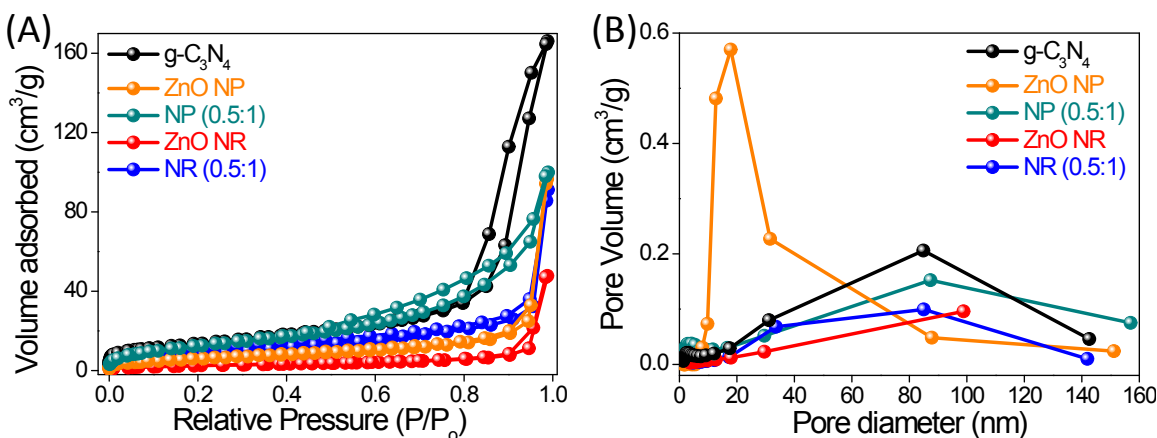
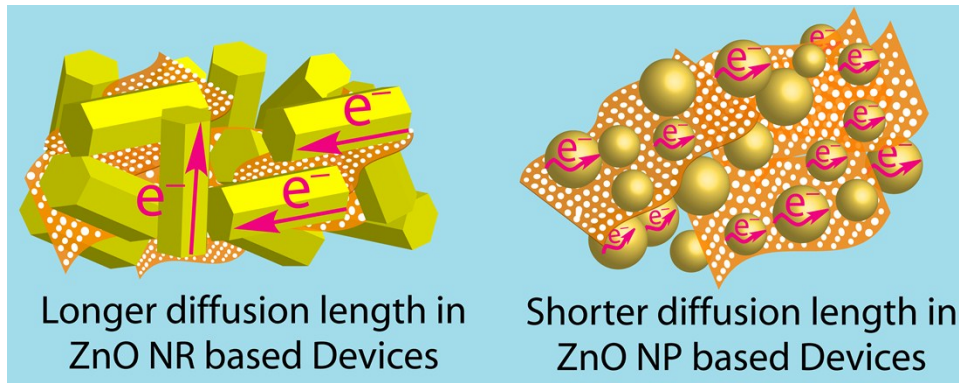


Figure S10. (A) Nitrogen adsorption–desorption isotherms and (B) Barrett–Joyner–Halenda (BJH) pore size distribution plots for as synthesized pristine g-C₃N₄ (Black line), ZnO NP (Orange line), ZnO NR (Red line) and composites namely, NP(0.5:1) [dark cyan line], and NR(0.5:1) (Blue line).

Desired characteristics of a photoanodic material to be used in QDSSC devices in order to achieve better photovoltaic performance are: it should have (i) a high surface area and (ii) highly porous in nature. Type IV isotherms with H3 hysteresis loops are observed for as synthesized g-C₃N₄, ZnO NPs and also for both the composites which confirm mesoporous characteristic of the materials. The observed BET surface area values for all the as-synthesized materials are: 78 m²g⁻¹ for g-C₃N₄, 36 m²g⁻¹ for ZnO NP, 48 m²g⁻¹ for composite NP (0.5:1), 16 m²g⁻¹ for ZnO NR, and 30 m²g⁻¹ for composite NR (0.5:1). There, the values of BET surface area for ZnO NP and its g-C₃N₄ composite [i.e., NP (0.5:1)] are found to be higher than their counterparts; ZnO NR and NR (0.5:1) respectively. This observation is in accordance with the diffuse reflectance UV-vis analyses for CdS QD sensitized photoanodes; wherein, a higher loading of CdS QDs is noted in the ZnO NP based photoanodes. So, it is confirmed that due to higher specific surface area provided by the ZnO NPs, CdS QDs are quantitatively loaded more in ZnO NP photoanodes. Moreover, it should be noted that the BET surface area value is higher for as synthesized g-C₃N₄ sheets among all the materials and with the addition of it to the composite the specific surface area is also increases.

From the BJH pore size distribution curves, pore distribution in pristine ZnO NPs is observed to be in the range of (15–50) nm while for the other materials namely, g-C₃N₄, NP (0.5:1) composite, NR (0.5:1) composite are in the range of (30–120) nm. There is no indication of pores in case of pristine ZnO NRs.

10. Scheme S1. Comparison of electron transport in CdS sensitized (g-C₃N₄-ZnO NR) and (g-C₃N₄-ZnO NP) photoanodes.



Scheme S1 shows longer diffusion length of photoinduced electrons in ZnO NR based photoanodes as compared to the ZnO NP photoanodes which is due to the larger size of single crystalline ZnO NRs.

11. Table S3. An overview of the present scenario of **ZnO Based CdS sensitized** solar cells and their relevant performance parameters along with our results in the present manuscript

Ref No.	ZnO Nanostructures	J_{sc} (mA/cm ²)	V_{oc} (mV)	FF (%)	η (%)	Active Area (cm ²)	Counter Electrode
SI 7	ZnO-CdS-GO	7.3	703	54.6	2.8	1.2	Pt/FTO
SI 8	ZnO NWs	5.42	580	34	1.1	No data	Pt/FTO
SI 9	ZnO NW/Zn ₂ SnO ₄	3.68	760	44	1.3	0.25	Pt/FTO
SI 10	ZnO NW/ZnO HMSP	9.01	511	51	2.4	1	Pt/FTO
SI 11	Porous ZnO NS	7.9	520	30	1.16	0.25	Pt/FTO
Present work	ZnO NR-C ₃ N ₄	11.1	650	34	2.43	0.5	Pt/FTO

REFERENCES

- (SI 1) S. Kumar, A. Baruah, S. Tonda, B. Kumar, V. Shanker and B. Sreedhar, *Nanoscale*, 2014, **6**, 4830–4842.
- (SI 2) Y.J. Wang, R. Shi, J. Lin and Y.F. Zhu, *Energy Environ. Sci.*, 2011, **4**, 2922–2929.
- (SI 3) D. Wu, K. Cao, F. Wang, H. Wang, Z. Gao, F. Xu, Y. Guo and K. Jiang, *Chem. Eng. J.*, 2015, **280**, 441–447.
- (SI 4) P. Fageria, R. Nazir, S. Gangopadhyay, H. C. Barshilia and S. Pandea, *RSC Adv.*, 2015, **5**, 80397–80409.
- (SI 5) H. Zeng, G. Duan, Y. Li, S. Yang, X. Xu and W. Cai, *Adv. Funct. Mater.*, 2010, **20**, 561–572.
- (SI 6) X. L. Wu, G. G. Siu, C. L. Fu and H. C. Ong, *Appl. Phys. Lett.*, 2001, **78**, 2285–2287.
- (SI 7) D. Barpuzary and M. Qureshi, *ACS Appl. Mater. Interfaces*, 2013, **5**, 11673–11682.
- (SI 8) C.-Z. Yao, B.-H. Wei, L.-X. Meng, H. Li, Q.-J. Gong, H. Sun, H.-X. Ma and X.-H. Hu, *J. Power Sources*, 2012, **207**, 222–228.
- (SI 9) T. Bora, H. H. Kyaw, J. Dutta, *Electrochim. Acta*, 2012, **68**, 141–145.
- (SI 10) T. R. Chetia, D. Barpuzary and M. Qureshi, *Phys. Chem. Chem. Phys.*, 2014, **16**, 9625–9633.
- (SI 11) H. Chen, W. Li, H. Liu and L. Zhu, *Electrochem. commun.*, 2011, **13**, 331–334.